

CrossTremor: An Automatic Detection Code of Tremors with Tectonic Earthqukes as Green's Functions

Carlos Ramírez Piña[1], Ricardo Vazquez Rosas[2], J. A. Hernández-Servín[1(✉)], and Gerardo León Soto[2(✉)]

[1] Facultad de Ingeniería, Universidad Autónoma del Estado de México, Toluca, Estado de México, Mexico
joseph_servin@uaemx.mx

[2] Facultad de Arquitectura, Universidad Michoacana de San Nicolás de Hidalgo, Morelia, Michoacán, Mexico
gleon@umich.mx

Abstract. CrossTremor a cross correlation code for detecting seismic tremors is presented. The code uses tectonic earthquakes as Green's functions to identify non volcanic seismic tremors. A six steps methodology is proposed: Downloading the continuous recording by day, obtaining the response files and removing the instrument response of the data, identification of candidate tremors, extraction of candidate tremors, moment magnitude computation, and seismic site effects estimation. As a case of study, CrossTremor is applied to one year data (2006) of CODEX and MARS temporal seismic arrays in western Mexico. The code identified 530 non vocanic tremors in this region with moment magnitudes ranged from 3.3 to 5.0 with respective corner frequencies from 1.1 to 7.3 Hz. Estimated fundamental periods were computed in a range of 1.0 to 10.3 Hz. CrossTremor is an open software available in the GitLab repository https://gitlab.com/cramirezp/crosstremors.git.

1 Introduction

After the 1906 San Francisco earthquake ($M > 7.9$, [1,2]), H.F. Reid proposed the *Elastic Rebound Theory* to explain earthquakes [3]. The Elastic Rebound Theory basically states that elastic strain is accumulated over a geological fault locked by friction. When the strain reaches certain treshold, all the accumulated energy is suddenly released and a part of this energy is radiated away as seismic waves. Events generated by this mechanism are referred to as *tectonic earthquakes*. Tectonic earthquakes were one of the main sources of information of the Earth structure along the XX century. However, "slow earthquakes" were reported near of the end of the 1990s and the beggining of this century. A *Slow slip event*, with a duration of 300 days, was reported in the Japan subduction zone after two large earthquakes in 1996 [4]. *Nonvolanic tremors* with duration of a few weeks were also observed in southwest Japan in 2001 [5]. After that,

© The Author(s), under exclusive license to Springer Nature Switzerland AG 2024
R. Silhavy and P. Silhavy (Eds.): CSOC 2024, LNNS 1118, pp. 327–339, 2024.
https://doi.org/10.1007/978-3-031-70285-3_24

slow earthquakes have been observed in a number of tectonic settings such as Alaska [6], Cascadia [7], Mexico [8], Costa Rica [9], and California [10].

As tectonic earthquakes, slow earthquakes are nucleated in faults, but they are generated above or below the seismogenic zone, i.e. above or below the zone where tectonic earthquakes are produced. In contrast with tectonic earthquakes which are nucleated by fast coseismic slip, slow earthquakes are related to stable sliding along the interface of the fault [11]. Low-frequency earthquakes (LFEs) are slow earthquakes that exhibit predominant frequencies in the range of 1–10 Hz which are lower than the frequencies in a tectonic earthquake. Tremors are a superposition of swarms of LFEs [12].

The use of tectonic earthquakes as empirical Green's functions for LFEs has been proposed by Thomas *et al.*. [13]. Since tremors are generated by swarms of LFEs [12], tectonic earthquakes may be used as seeds of a tremor provided that they are close to the source of the tremor, the time duration of the tectonic earthquake is short relative to the tremor duration, and both events have similar source mechanisms [13].

2 Methodology

A methodology to detect tremors with dominant frequencies between 1 and 10 Hz is proposed [14]. This method uses wavefronts from seismic events below the seismogenic zone (depths between 29 and 50 km). The seismic events are previously known and they are called *master events* or *tempíates*. Six steps are proposed: Downloading the continuous recording by day, obtaining the response files and removing the instrument response of the data, identification of candidate tremors, extraction of candidate tremors, moment magnitude computation, and seismic site effects estimation.

2.1 Downloading of Contiuous Recording by Day

The code is designed to download recordings by day from the Seismological Facility for the Advance of Geoscience (SAGE) repositories. Input information is network code assigned by SAGE, station names, year, month, channel, and starting day of downloading. These information can be consulted in the SAGE webpage (www.iris.edu). The dowloaded daily recordings are saved in the Seismic Analysis Code format (SAC) [15] and stored in a directory named by the network code and classified by Julian day.

2.2 Obtaining the Response Files and Removing the Instrument Response

The code download the response files and remove the instrument response to the raw data. Removing the instrument response is an important step in preprocessing because the raw data are strongly affected by the type of seismic sensor. The effect of the sensor to the recorded data can be removed and the technical

information of the sensor (poles and zeros) is specified in the response files. The response files can be downloaded from the SAGE repositories by specifying the network code, station names, channel, and operating date. The response files are stored in a directory with the name of the code of the station.

The raw data are corrected for the instrument response with utilities of the Seismic Analysis Code [15]. Raw data are reported by default as velocity recordings. In the correction process, the raw data are also converted to displacement recordings.

2.3 Identification of Candidate Events

The method proposes previously located tectonic earthquakes as Green's functions of non volcanic tremors. Green's functions act as unit response of the medium to build up tremors. These tectonic events act as templates for identifying larger tremors by cross correlation in the frequency domain. It is assumed that the preprocessing of the templates is the same as the downloaded data described in Sect. 2.2. It is only considered the vertical component of events nucleated below the seismogenic zone where non volcanic tremors have been typically observed (between 29 and 50 km depth).

The vertical component of each template, $u(t)$, is cross correlated with the vertical component of the data of a day of recording, $v(t)$, at the corresponding seismic station. Data of a day is divided in 20 disconected time intervals, $v_i(t)$, covering the entire day. A fast Fourier transform is applied to the template $u(t)$ and the time interval $v_i(t)$ to obtain the frequency spectra $U(f)$ and $V_i(f)$, respectively. In the frequency domain, the cross correlation, $C_i(f)$, of $U(f)$ and $V_i(f)$ is defined by

$$C_i(f) = U^*(f)V_i(f) \tag{1}$$

Each frequency window $V_i(f)$ is cross correlated as a data streaming over the template in the frequency domain $U(f)$. Cross correlations greater than 0.8 are marked for extraction.

2.4 Extraction of Candidate Events

Cadidate events detected in step 2.3 are classified by waveform template whose size is specified by the user. An automatic picker is used for grouping detected stations in its three channels. Since typically there is no clear P or S arrivals, this procedure is semiautomatic and the user needs visually check the tremor.

2.5 Moment Magnitude Computation

In order to quantify the size of the tremor, the *magnitude moment*, M_w, is computed. The moment magnitude can be estimated from the energy release or *seismic moment* M_0, the *corner frequency* of the spectrum f_c, and the *stress drop* of the slip $\Delta\sigma$ [16]. The corner frequency can be defined as the frequency below that it is concentrated most of the energy in displacement recordings [17].

The stress drop, $\Delta\sigma$, is the change in stress during the event and is assumed independent from the seismic moment [16]. Under the Brune [18,19] model and assuming that the corner frequency is inversely proportional to the cubic root of the seismic moment [20], the relation among f_c, M_0, and $\Delta\sigma$ is given by [18,19]

$$f_c = 4.91 \times 10^6 \beta \left(\frac{\Delta\sigma}{M_0} \right)^{1/3} \tag{2}$$

where β is the shear wave velocity in km/s, the stress drop $\Delta\sigma$ is measured in bars, the corner frequency f_c is in Hertz, and the seismic moment is in $dyne\,cm$ [21]. Once the seismic moment is obtained, the moment magnitude is computed by the relation [22]

$$M_w = \frac{\log_{10} M_0}{1.5} - 6.07 \tag{3}$$

2.6 Seismic Site Effect Estimation

Crosstremor computes the seismic site effect at the station location from the detected tremors. Seismic site effect is the ground response due to local geological conditions. It is characterized by the fundamental frequency (or fundamental period) of the ground. The Nakamura method [23] is based on finding the maximum energy from the ratio H/V, where H indicates the horizontal components and V the vertical component of the seismic recording in the frequency domain

$$\frac{H}{V} = \sqrt{\frac{\sum_{n=1}^{N} (NS_n^2 + EW_n^2)}{\sum_{n=1}^{N} V_n^2}} \tag{4}$$

where NS_n, EW_n, and V_n are the discrete spectra in the North-South, East-West, and vertical components, respectively. N is the number of discrete frequencies. The frequency that maximizes the value of H/V corresponds to the fundamental frequency.

2.7 Dataset

Seismic tremors have been observed in western Mexico [8] which is a subduction tectonic environment where the oceanic Cocos and Rivera plates subduct beneath the continental North American plate (Fig. 1). The Rivera and Cocos plates have independent motions since 10 Ma [24]. The Rivera and Cocos plates are separated offshore by El Gordo Graben (GG). The coupling of the subducting plates to the continental North American plate and the differential motion between the Rivera and Cocos plates produces the formation of the Colima Rift (CR) [25]. The Colima Rift separates the tectonic units known as the Jalisco Block and the Michoacan Block.

The dataset was provided by Colima Deep Experiment (CODEX) [26] and the Mapping of the Rivera Subduction Zone (MARS) [27] temporal experiments in

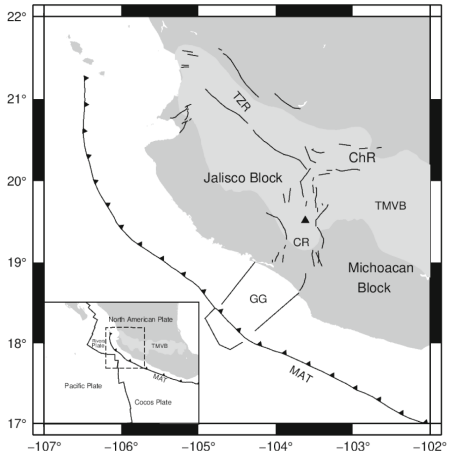


Fig. 1. Tectonic enviroment of western Mexico. Light gray denotes the Trans-Mexican Volcanic Belt (TMVB). The strike of the boundary of the subducting plates is represented by the line with triangles known as the Middle Ametican Trench (MAT). The triangles orientation denotes the direction of the subduction. GG stands for El Gordo Graben, TZR for Tepic-Zacoalco Rift, CR for Colima Rift, and ChR for Chapala Rift.

western Mexico. CODEX experiment consisted of 22 broadband seismic stations around the Colima volcanic complex recording data between 2006 and 2008 at a sampling rate of 100 Hz. MARS array was a deployment of 50 broadband stations installed across the Jalisco and Michoacan blocks between January 2006 and may 2007 at a sampling rate of 40 Hz (see Fig. 2). The master events were relocated earthquakes from the catalog reported by Ramírez-Piña *et al.* [28]. A total of 678 master events were used as Green's functions of tremors (Fig. 3).

3 Results

The results of the code to the test dataset is presented at each step of the methodology.

3.1 Downloading of Contiuous Recording by Day

The test dataset and additional information is provided by SAGE. In the case of the CODEX experiment, the assigned code network is ZA, stations names (ALPI, BAVA, CANO, CDGZ, COLM, COMA, CUAT, EBMG, ESPN, GARC, HIGA, JANU, MAZE, MORA, OLOT, PAVE, PERC, SANM, SCRI, SINN, SNID, ZAPO), years (2006, 2007), month (January to December each year), channels (HHZ, HHN, HHE). For MARS array, the code netwrok is XF, stations (MAXY, where XY is a number between 01–55), years (2006, 2007), months (January 2006 to May 2007), channels (BHZ, BHN, BHE). The starting day is defined by the user.

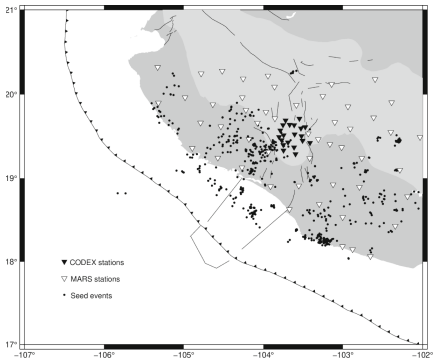


Fig. 2. Map showing the seismic stations of CODEX and MARS experiments (inverted black and white triangles, respectively). Epicenters of master events are marked by black circles.

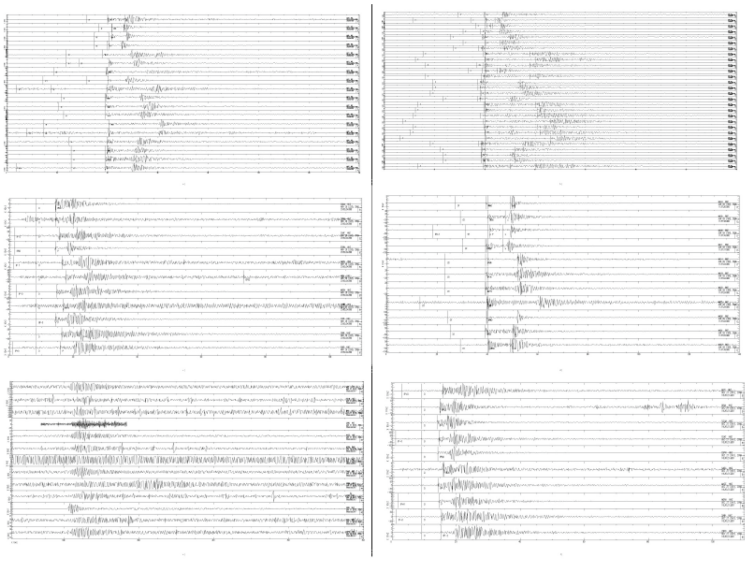


Fig. 3. Examples of tectonic events used as templates.

3.2 Obtaining the Response Files and Removing the Instrument Response

Crosstremor can download the response files from SAGE repositories by introducing the information of the experiments as in Sect. 3.1. If the user already have the response files, the code can read them by indicating where they are stored. The correction for the instrument response of the downloaded data is automatically done with SAC utileries. The final output are the data organized by day, with the response corrected, and in units of displacement in nm.

3.3 Identification of Candidate Events

The cross correlation module is used to test the code with 53 master events. These master events were events reported by [28] and relocated with a double difference algorithm [29] (see the GitLab repository for additional information https://gitlab.com/cramirezp/crosstremors.git).

CrossTremor looks for correlated signals with the master events in the vertical component. It is set a correlation threshold of 0.8 and it is required a minimum of three stations to define a candidate event. It was used data from 2006 of CODEX and MARS experiments. A total of 15485 signals with the specified parameters were identified giving a total of 530 tremors. Figure 4 shows some detected candidate tremors.

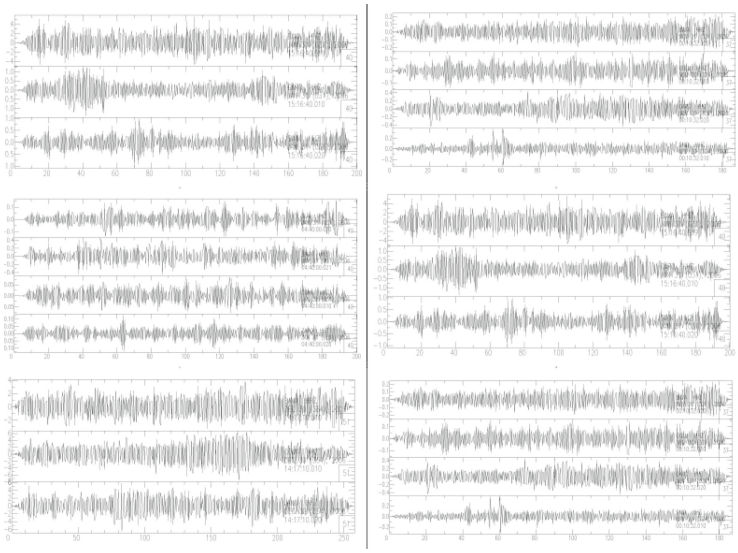


Fig. 4. Examples of tremor candidates detected by the code.

3.4 Extraction of Candidate Events

Candidate events are selected and stored in directories. At this step a visual checking by an analist is needed to discard noisy records or non temor detections. CrossTremor detects high cross correlation signals, including tectonic events. If tectonic events are not of interest, they need to be discarded manually.

3.5 Moment Magnitude Computation

An estimation of the corner frequency is needed to compute the moment magnitude. The corner frequency is estimated by the corner frequency module. Figure 5 shows some examples of the cerner frequency estimation. Most of the energy is in the flat region of the spectrum (at low frequencies). The corner frequency is identified as the inflection frequency where the amplitude spectrum decays to lower values.

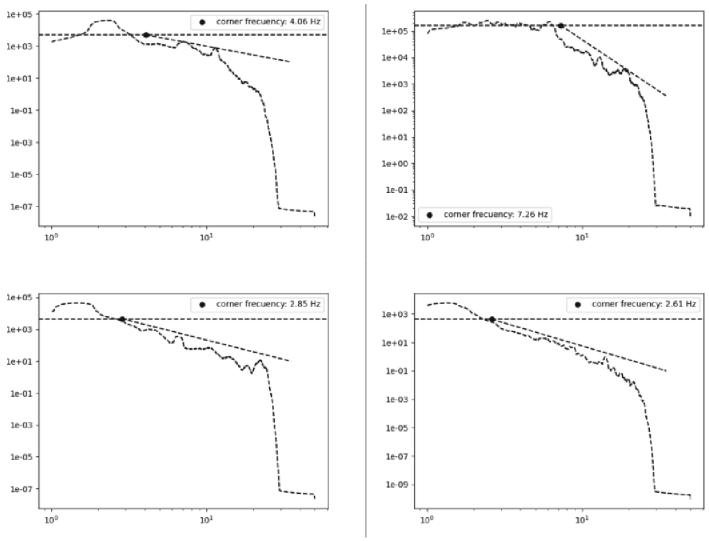


Fig. 5. Examples of estimation of corner frequencies.

Seismic moment is estimated from equation (2) with local parameters: a shear velocity of 3.4 km/s [30] and a constant stres drop of $\Delta\sigma = 100\,bars$. The corner frequency modulus creates an archive named "corner_frequency" in which each selected recording is stored. The station, the corner frequency, and the number of incidences are kept as shown in Table 1.

Table 1. Output results from the test data set. M_0 stands for the *seismic moment*, f_c for the *corner frequency* of the spectrum, M_w is the moment magnitude, N_0 is the number of events detected as a function of the corner frecuency.

M_0	f_c	M_w	N_0	M_0	f_c	M_w	N_0	M_0	f_c	M_w	N_0
3.19E+023	1.1	5	1	1.42E+022	3.1	4.1	18	3.40E+021	5	3.6	3
2.46E+023	1.2	4.9	2	1.26E+022	3.2	4	23	3.20E+021	5.1	3.6	3
1.55E+023	1.4	4.8	3	1.18E+022	3.3	4	20	3.025E+021	5.2	3.6	5
1.26E+023	1.5	4.7	3	1.08E+022	3.4	4	29	2.85E+021	5.3	3.6	7
1.03E+023	1.6	4.6	27	9.92E+021	3.5	4	19	2.70E+021	5.4	3.6	3
8.65E+022	1.7	4.6	27	9.11E+021	3.6	3.9	19	2.55E+021	5.5	3.6	5
7.29E+022	1.8	4.5	21	8.39E+021	3.7	3.9	15	2.42E+021	5.6	3.5	8
6.20E+022	1.9	4.5	26	7.75E+021	3.8	3.9	24	2.29E+021	5.7	3.5	7
5.31E+022	2	4.4	9	7.17E+021	3.9	3.9	17	2.18E+021	5.8	3.5	7
4.59E+022	2.1	4.4	5	6.64E+021	4	3.8	13	2.07E+021	5.9	3.5	7
3.99E+022	2.2	4.4	4	6.17E+021	4.1	3.8	8	1.96E+021	6	3.5	4
3.49E+022	2.3	4.3	2	5.74E+021	4.2	3.8	9	1.87E+021	6.1	3.5	3
3.07E+022	2.4	4.3	2	5.35E+021	4.3	3.8	15	1.78E+021	6.2	3.5	3
2.72E+022	2.5	4.2	5	4.99E+021	4.4	3.8	5	1.62E+021	6.4	3.4	4
2.42E+022	2.6	4.2	6	4.66E+021	4.5	3.7	7	1.54E+021	6.5	3.4	3
2.16E+022	2.7	4.2	4	4.37E+021	4.6	3.7	7	1.41E+021	6.7	3.4	4
1.93E+022	2.8	4.1	6	4.09E+021	4.7	3.7	11	1.35E+021	6.8	3.4	1
1.74E+022	2.9	4.1	11	3.84E+021	4.8	3.7	8	1.29E+021	6.9	3.4	3
1.57E+022	3	4.1	14	3.61E+021	4.9	3.7	3	1.09E+021	7.3	3.3	2

3.6 Seismic Site Effect Estimation

Crosstremor computes the H/V values giving the names of the stations to be analyzed. The archive with stations names needs to be stored in the path where the tremors catalog is saved. The code generates an archive with the H/V data as illustrated in Fig. 6. The spatial distribution of H/V values are srtored in a different archive. Table 2 gives the values of the fundamental frequency (and fundamental period) at each station and Fig. 7 shows some fundamental frequencies as red circles.

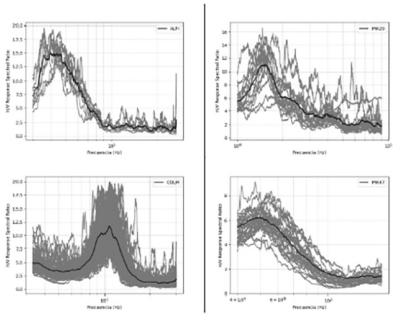


Fig. 6. H/V response spectral ratios for the ALPI, MA29, COLM and MA47 stations. Gray lines are the H/V ratios of all the ground motions recorded in the statios and in black the 50th percentile.

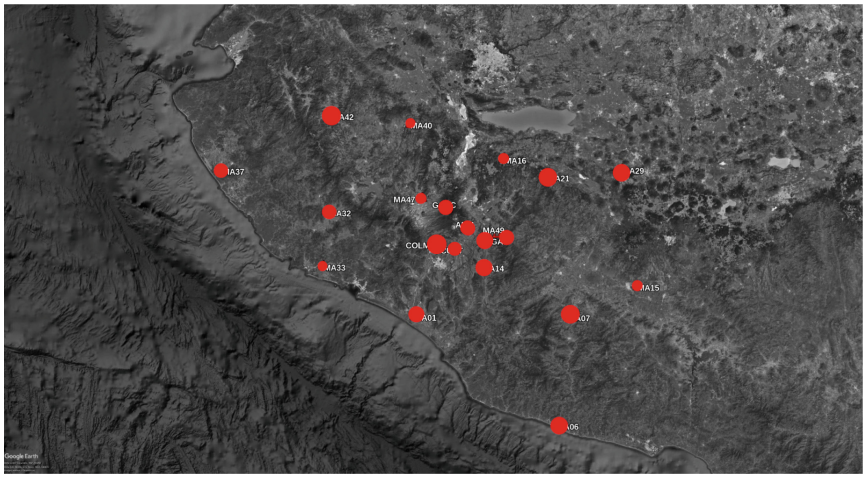


Fig. 7. Spatial distribution of fundamental frequencies at station locations. The size of the circles are scaled according to the fundamental frequency.

Table 2. values computed H/V by stations

Station	H/V(Hz)	T(s)	Latitude	Longitude
ALPI	4.0	0.3	19.5027	−103.5218
COLM	10.3	0.1	19.3975	−103.7503
CUAT	3.7	0.3	19.3682	−103.6148
GARC	4.4	0.2	19.6383	−103.6705
HIGA	5.3	0.2	19.4226	−103.4153
MA01	5.0	0.2	18.9014	−103.9112
MA06	5.8	0.2	18.1461	−102.8798
MA07	7.3	0.1	18.8933	−102.7943
MA14	5.8	0.2	19.2385	−103.4190
MA15	1.1	0.9	19.0985	−102.2863
MA16	1.1	0.9	19.9778	−103.2540
MA21	8.8	0.1	19.8540	−102.9380
MA29	6.5	0.2	19.9038	−102.3900
MA32	4.0	0.3	19.6162	−104.5338
MA33	1.0	1.0	19.2432	−104.5723
MA37	4.0	0.3	19.8990	−105.3185
MA40	1.0	1.0	20.2198	−103.9420
MA42	9.1	0.1	20.2777	−104.5175
MA47	1.1	0.9	19.7118	−103.8553
MA49	4.4	0.2	19.4638	−103.3109

4 Discussion

CrossTremor is a code to detect tremors from a set of tectonic earthquakes acting as Green's functions. It is assumed that the waveforms of the master events are available. These waveforms can be downloaded from SAGE respositories or be obtained from a local seismological service. The code downloads the time series by day and the response files from SAGE servers, correct for the instrument response, and convert the data to displacement. After that, it cross correlates the master events with the corrected time series in the frequency domain and looks for correlations greater than 0.8. The coincidences are selected and stored in individual directories. Finally, corner frequencies, seismic moments, moment magnitudes, and site effects are estimated.

As a case of study, the code was applied to western Mexico, where tremors have been previously reported [8]. CrossTremor was able to successfully identify 530 non vocanic tremors in this region. Moment magnitudes ranged from 3.3 to 5 with respective corner frequencies from 1.1 to 7.3 Hz.

An advantage of the code is that provides the site efects at the location of the stations from non volcanic tremors. Fundamental periods ranged from 1.0

to 10.3 Hz. Provided that the region of study presents tremors, the site effects can be determined from this information with no information of tectonic events or strong motion measurements. This information is valuable in seismic hazard and risk analysis and seismic engineering.

CrossTremor is an open source code now available in the GitLab repository https://gitlab.com/cramirezp/crosstremors.git.

Acknowledgment. This work has received partial support from the Mexican CONACHYT through the Student Support Program [CVU 702528]. We express our gratitude to the 'Mandra' Digital Innovation Center, located at the Faculty of Sciences of the Autonomous University of the State of Mexico, for providing facilities essential to the completion of this research. Some of the figures were made with Generic Mapping Tools [31].

References

1. Wald, D.J., Kanamori, H., Helmberger, D., Heaton, T.H.: Source study of the 1906 San Francisco earthquake. Bull. Seis. Soc. Am. **83**, 981–1019 (1993)
2. Song, S.G., Beroza, G.C., Segall, P.: A unified source model for the 1906 San Francisco earthquake. Bull. Seis. Soc. Am. **98**, 823–831 (2008)
3. Reid, H.F.: The Mechanics of the Earthquake, The California Earthquake of April 18, 1906, Report of the State Investigation Commission, vol. 2. Carnegie Institution of Washington, Washington, D.C. (1910)
4. Hirose, H., Hirahara, K., Kimata, F., Fujii, N., Miyazaki, S.: A slow thrust slip event following the two 1996 Hyuganada earthquakes beneath the Bungo Channel, southwest Japan. Geophys. Res. Lett. **26**, 3237–3240 (1999)
5. Obara, K.: Nonvolcanic deep tremor associated with subduction in southwest Japan. Science **296**, 1679–1681 (2002)
6. Ohto, Y., Freymueller, J.T., Hreinsdóttir, S., Suito, H.: A large slow slip event and the depth of the seismogenic zone in the south central Alaska subduction zone. Earth Planet. Sci. Lett. **247**, 108–116 (2006)
7. Miller, M.M., Melourne, T., Johnson, D.J., Summer, W.Q.: Periodic slow earthquakes from the Cascadia subduction zone. Science **295**, 2423 (2002)
8. Brudzinski, M.R., et al.: Tectonic tremor and slow slip along the northwestern section of the Mexico subduction zone. Earth Planet. Sci. Lett. **454**, 259–271 (2016)
9. Walter, J., Schwartz, S., Protti, M., Gonzalez, V.: The synchronous occurrence of shallow tremor and very low frequency earthquakes offshore of the Nicoya Peninsula, Costa Rica. Geophys. Res. Lett. **40**, 1517–1522 (2013)
10. Shelly, D.R., Hardebeck, J.L.: Precise tremor source locations and amplitude variations along the lower-crustal central San Andreas Fault. Geophys. Res. Lett. **37**, L14301 (2010)
11. Obara, K.: Characteristic activities of slow earthquakes in Japan. Proc. Jpn. Acad. Ser. B **96**, 297–315 (2020)
12. Shelly, D.R., Beroza, G.C., Ide, S.: Non-volcanic tremor and low-frequency earthquake swarms. Nature **446**, 305–307 (2007)
13. Thomas, A.M., Beroza, G.C., Shelly, D.R.: Constraints on the source parameters of low-frequency earthquakes on the San Andreas Fault. Geophys. Res. Lett. **43**, 1464–1471 (2016)

14. Nishikawa, T., Ide, S., Nishimura, T.: A review on slow earthquakes in the Japan Trench. Progr. Earth Planetary Sci. 1–51 (2023)
15. Goldstein, P., Snoke A.: SAC availability for the IRIS community. Incorporated Institutions for Seismology Data Management Center Electronic Newsletter (2005)
16. Stein, S., Wysession, M.: An Introduction to Seismology, Earthquakes, and Earth Structure. Blackwell Publishing (2003)
17. Kramer, S.: Geotechnical Earthquake Engineering. University of Washington (1996)
18. Brune, J.N.: Tectonic stress and the spectra of seismic shear waves from earthquakes. J. Geophys. Res. **75**, 4997–5009 (1970)
19. Brune, J.N.: Correction [to "tectonic stress and the spectra of seismic shear waves from earthquakes". J. Geophys. Res. **76**, 5002 (1971)
20. Michel, S., Gualandi, A., Avouac, J.P.: Similar scaling laws for earthquakes and Cascadia slow-slip events. Nature **574**, 522–526 (2019)
21. Boore, D.M.: Stochastic simulation of high-frequency ground motions based on seismological models of theradiated spectra. Bull. Seis. Soc. Am. **73**, 1865–1894 (1983)
22. Havskov, J., Ottemöller, L.: Routine Data Processing in Earthquake Seismology. Springer, Heidelberg (2010). https://doi.org/10.1007/978-90-481-8697-6
23. Nakamura, Y.: A method for dynamic characteristics estimation of subsurface using microtremor on the ground surface. Quaternary Rep. Railw. Tech. Res. Inst. **30**, 25–33 (1989)
24. DeMets, C., Traylen, S.: Motion of the Rivera plate since 10Ma relative to the Pacific and North American plates and the mantle. Tectonophysics **318**, 119–159 (2000)
25. Bandy, W., Mortera-Gutierrez, C., Urrutia-Fucugauchi, J., Hilde, T.W.C.: The subducted Rivera-Cocos Plate boundary: where is it, what is it, and what is its relationship to the Colima rift? Geophys. Res. Lett. **22**, 3075–3078 (1995)
26. West, M.: The Colima deep seismic experiment: imaging the magmatic root of colima volcano [data set]. Int. Fed. Digit. Seismogr. Netw. (2006)
27. Grand, S., Ni, J.: Mapping the Rivera subduction zone [data set]. Int. Fed. Digit. Seismogr. Netw. (2006)
28. Ramírez-Piña, C., Escudero, C.R., Hernández-Servín, J.A., León Soto, G.: CrossQuake: a cross-correlation code for detecting small earthquakes in the frequency domain. In: Silhavy, R., Silhavy, P. (eds.) CSOC 2023. LNNS, vol. 722, pp. 488–497. Springer, Cham (2003). https://doi.org/10.1007/978-3-031-35311-6_49
29. Waldhauser, F., Ellsworth, W.L.: A double-difference earthquake location algorithm: method and application to the northern hayward fault, California. Bull. Seism. Soc. Am. **90**, 1353–1368 (2000)
30. Gómez-González, J.M., Mendoza, C., Sladen, A., Guzmán-Speziale, M.: Kinematic source analysis of the 2003 Tecomán, México, earthquake (Mw 7.6) using teleseismic body waves. Bol. Soc. Mex. **62**, 249–262 (2010)
31. Wessel, P., et al.: The generic mapping tools version 6. Geochem. Geophys. Geosyst. **20**, 5556–5564 (2019)



Application for Monitoring Sentiment Analysis and Geolocation in Shared Vehicle Services

Christian Ovalle(✉)

Universidad Tecnológica del Perú, Lima, Perú
dovalle@utp.edu.pe

Abstract. The research was oriented toward creating a cutting-edge application that uses sentiment analysis and geolocation to improve safety in shared vehicle services. The objectives outlined ranged from designing the application to share emotional states and locations in real-time to evaluate the accuracy of the incident detection system, comparing its effectiveness, and conducting pilot tests in real-life situations. Implementing the Convolutional Neural Network (CNN) model emerged as a core component, resulting in 74% accuracy in sentiment classification. The findings highlighted the system's effectiveness in achieving remarkable recall rates, especially in categories such as calm (78%) and noise (81%). However, limitations were identified in the accuracy of certain emotional states, such as sadness (40%). Despite these limitations, the conclusions emphasize the success in achieving the objectives, highlighting the application's usefulness for improving citizen security. Continuous improvements in the model, institutional collaborations to strengthen its integration into security systems, and educational campaigns for users focusing on ethics and privacy are proposed. In summary, the research provides a robust basis for future developments, highlighting the optimization and adaptability of the application in diverse urban environments.

Keywords: Convolutional neural network · Speech sentiment analysis · Mobile application · Artificial intelligence · Security in-vehicle services

1 Introduction

Artificial intelligence (AI) has increased enormously in recent years, giving machines or AIs the power to learn and make decisions in various industries, such as security [1]. However, as AI plays a more critical role, it is essential to explore how the information provided by AI influences the user's decision [2]. In this sense, from a security perspective, decision-making based on AI will depend mainly on its reliability and accuracy [3]. Likewise, given this proliferation of emerging technologies, vehicles become part of an intelligent transportation system (ITS), where their development, together with technologies such as the Internet of Things (IoT), generates an improvement in transportation systems [4]. Given this, IoT and Radio Frequency Identification (RFID) systems in ITS have proven to be essential for the safety and efficiency of transportation [5].

Consequently, new applications capable of tracking vehicles in real-time and triggering location-based alerts have been contributing to safeguarding the lives of citizens

© The Author(s), under exclusive license to Springer Nature Switzerland AG 2024
R. Silhavy and P. Silhavy (Eds.): CSOC 2024, LNNS 1118, pp. 340–354, 2024.
https://doi.org/10.1007/978-3-031-70285-3_25

[6]. At the same time, location monitoring has become a way to ensure safe travel [7], since viewed from various situations and in conjunction with technologies such as RFID (Radio Frequency Identification) and IoT [8], it is possible to detect anomalous driving movements using this real-time global positioning data [9]. Moreover, considering AI and speech, it is possible to detect emotions that play a crucial role in diagnosing abnormal situations in citizen security [10]. That is why new approaches are generated using AI and based on frequency-modulated continuous wave radar that seeks to estimate a moving vehicle's location more accurately [11]. Therefore, safety in shared-vehicle services is at the center of attention due to complex challenges that require innovative approaches to ensure citizens' protection and peace of mind. It is a fact that reliability is one of the qualities that this type of transport service must provide [12]. Thus, factors such as the driver's attitude and age play an important role as an indicator of safety in this service [13]. However, it is essential to mention that criminal acts cannot be entirely prevented. However, they can be prevented by planning an environment where the possibilities of the event can be reduced [14], which is why a large number of developed countries choose to solve these problems through the use of technology and artificial intelligence [15], thus generating technological solutions that can be coupled to a security system [16], thus replacing old solutions that did not end up being efficient in the face of the continuing problem [17]. Furthermore, from a Peruvian perspective, between 2022 and 2023, it has been found that 12 out of every 100 inhabitants will be victims of money, wallet, and cell phone theft, being this the crime that has increased the most compared to previous years, according to INEI (National Institute of Statistics and Informatics) [18]. Consequently, we can mainly point out the great feeling of distrust of the population of Lima about citizen security and public transportation, with 79% and 64.5% dissatisfaction, respweectively [19]. Despite this, the need to commute daily using public transport services forces users to expose themselves to a series of situations that involve the risk of being victims of criminals on the prowl [20], where it is mainly women who tend to see these factors as determinants for their choice of transport to use [21]. Our research work represents an innovation in mobile applications designed for sentiment analysis and geolocation monitoring in the context of shared vehicular services. Inspired by advances in contextual systems using mobile applications to improve safety in local environments [16] and passenger perception and behavioral adaptation in public transportation [12], we have implemented a system that combines real-time sentiment analysis with accurate geolocation. This innovation will allow shared service users to feel safer and more confident in their journeys while offering increased protection in identified risk areas through intelligent geofencing, following the approach of real-time vehicle tracking systems with automated security algorithms [22]. Moreover, by leveraging artificial intelligence (AI) to recommend personalized services to users, our project aligns with the trend of AI-based recommendation and enforcement of public services in smart cities [15], which improves operational efficiency and overall user experience in shared mobility services.

Moreover, our proposal also relies on advanced sentiment analysis methods and models to understand user opinions and emotions in real-time, contributing to proactively detecting risk areas in shared mobility [23]. Thus, we have developed a user emotion recognition model for the safety monitoring shared vehicles in public community spaces,

aligning with the Internet safety approach to vehicles in public spaces [24]. This innovation opens up new opportunities to ensure safety and improve the quality of shared vehicle services, thus contributing to a more complete and safer mobility experience for users.

2 Related Word

The research [17] focuses on the utilization of Global Positioning System (GPS) and Global Navigation Satellite System (GLONASS) technology to provide an effective real-time tracking solution. Consequently, the research culminated in the creation of an innovative mobile application that helps prevent the loss of children, adults, and people with disabilities, marking a significant breakthrough in crowd management and safety in smart cities. Likewise, their contributions are undeniable, as they address a growing need for tracking solutions in crowded places, making a lasting and essential impact on advancing the field of people tracking through mobile applications. However, the need to address technical and ethical challenges related to privacy in people tracking could be detected through some criticisms. However, the research is a valuable contribution if the environment of its use is changed to one of citizen security in shared vehicular services and promoting the use of new technologies such as artificial intelligence.

On the other hand, the research [25] represented a crucial technological idea that sought to monitor the transport of patients in ambulances in a context where the need to avoid compromising people's health through massive contagion by COVID-19 was urgent. However, despite its importance in contributing to health protection measures, the research needs concrete results that limit the knowledge and feasibility of such implementations in different national contexts. On the other hand, this research leverages the use of existing technologies such as vehicle tracking via GPS, services such as Firebase for data maintenance in the cloud, Geofencing to limit the visibility of ambulances to police officers, and Google Maps to facilitate the visualization of the real-time location of ambulances. Despite this, its almost zero maintenance costs under good management and influence, given the importance of solutions, make it a technology that is under improvement about its security functions, and boosting current technologies, such as the use of artificial intelligence, could be a significant contribution to the improvement of meeting citizens' needs about their safety.

The case of the research [26] emphasizes the importance of guaranteeing the safety of children in transportation to and from school through a system based on radio frequency identification technology (RFID) that is capable of tracking and monitoring by parents through the bus and the different private vehicles that carry out this transportation. As a result, it effectively monitored children with accurate and real-time information, thus improving their supervision and follow-up. However, the use of RFID technology for this type of project involves a long list of challenges where considerations such as how expensive it can be, how limited it is in large areas, its durability in environments not suitable for its implementation, and problems related to electromagnetic interference stand out, the last mentioned being one of the problems encountered in the scenarios conducted.

In the context of the research [27], it is essential to highlight the relevance of sentiment analysis in social networks, where it is noted that around 500 million tweets are sent

daily, reflecting the magnitude of unstructured data on this platform. Although this study focuses on the Peruvian political arena, its focus on sentiment analysis on Twitter and the use of advanced natural language processing (NLP) techniques resulted in an impressive average accuracy of 90.61% in evaluating its model. These statistics underscore the importance of effectively addressing unstructured data and demonstrate how sentiment analysis can be a powerful tool for understanding public perception. While the contextual circumstances are different, the methodologies and strategies used in this article can serve as a solid benchmark for ongoing research, highlighting the importance of effectively applying sentiment analysis in decision-making and continuous improvement of shared services.

Similarly, research [28] noted that an approach represents a significant advance, as it addresses the complexity of interpreting human sentiment through various modalities, such as text, voice tones, and facial expressions. In a world increasingly oriented to online video platforms, where users express their emotions and opinions by posting videos, Multimodal Sentiment Analysis (MSA) has gained relevance. This approach seeks to detect the sentiments present in these videos by leveraging multiple input modalities, including text, audio, and video. The strength of MSA lies in its ability to capture different emotional aspects and provide complementary information, which improves the accuracy of sentiment analysis. Thus, the paper addresses this critical challenge by proposing effective methods, both generative and conjoint learning, to deal with uncertain missing modalities in multimodal sentiment analysis.

Also, in research [29], it is essential to highlight the importance of geolocation technologies and machine learning in managing critical situations such as the COVID-19 pandemic. Obtaining an approach that divides the workplace environment into locations, using user-centric dynamic clustering techniques and leveraging wireless parameters such as Wi-Fi basic service set identifiers (BSSIDs) and Wi-Fi received signal strength (RSSI). Having as experimental results, a natural working environment that supports the effectiveness of the system with an accuracy of 98.25% in indoor geolocation and 76% in construction geolocation, demonstrating its applicability and scalability in work contexts and potentially in the monitoring of shared vehicular services in times of crisis such as pandemic.

Finally, in research [30], a crucial aspect is focused on the accuracy of emotion recognition in the presence of noise in facial images. Convolutional Neural Networks (CNNs) emerge as a promising technology in this task, but their performance may deteriorate in the presence of noise. This promising approach is applied by combining noisy and noiseless images in hybrid datasets, which has shown encouraging results by achieving 79% test accuracy on hybrid noise datasets, overcoming the limitations of previous approaches. The paper also explores advanced denoising and edge detection techniques, which are critical components in improving the performance of CNN models in facial emotion recognition in noisy images.

3 Methodology

The solution starts with user 1, entering the application and starting a trip; from that moment, the application will initially make use of the microphone that is predetermined in each mobile device to perform the analysis of feelings following the CNN classification

model, which will be in entire operation until user 1 finishes his trip. This model will have the sole function of determining whether user 1 has feelings of fear or sadness that may indicate a criminal act. At the same time, the application will use the GPS location of user 1. However, it will start in a state of shutdown, so it will not be initially updated in the database. Now, suppose the model detects those feelings that indicate being in a criminal act by user 1. In that case, this will activate the danger alert, initially changing the status of the GPS location of user 1 to active, thus alerting and sharing its location with user 2, who can monitor from the same application where user 1 is located. At the same time, the application will generate an alert sent to the authorities where they can also, but with more capacity, promptly track the GPS location of user 1, as shown in Fig. 1.

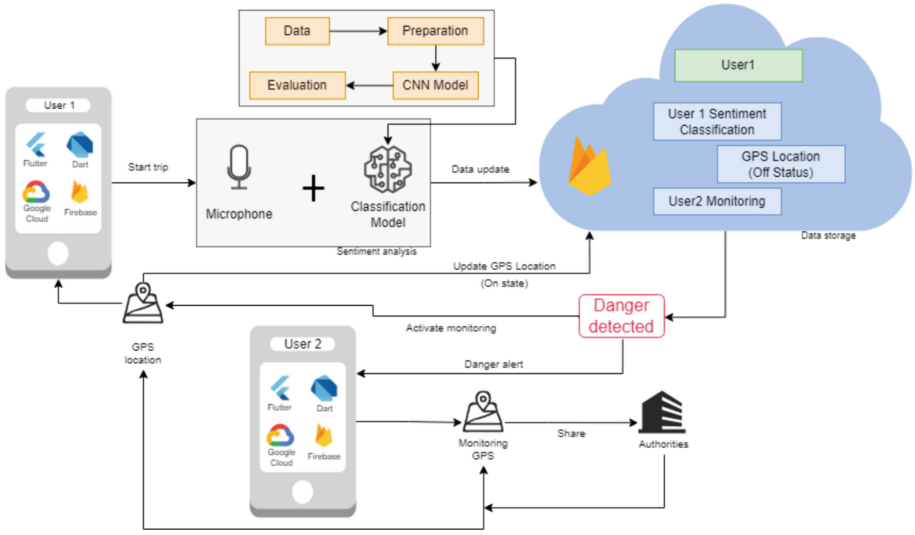


Fig. 1. Diagram of the proposed solution.

3.1 Development Methodology

We chose to follow the CRISP-DM (Cross-Industry Standard Process for Data Mining) methodology, which is widely recognized in machine learning and data mining but adapts well to solutions like the one presented here. frCRISP-DM comprises six phases: business understanding, data understanding, data preparation, modeling, evaluation, and deployment. However, in order to focus only on the stages directly related to the development of the convolutional neural network model and its subsequent deployment, it has been decided to adopt the methodology, finally having the following stages to follow: understanding the data, data preparation, modeling, evaluation and finally deployment.